Interplanetary Low-Thrust, Gravity-Assist Trajectory Design Using Resonant Orbits

Shanshan Pan [(1)], Mai Bando [(1)], Yang Wang [(2)]

[(1)] *Department of Aeronautics and Astronautics, Kyushu University*
Fukuoka, Japan
Email: shanshan.pan@aero.kyushu-u.ac.jp; mbando@aero.kyushu-u.ac.jp

[(2)] *School of Astronomy and Space Science, Nanjing University*
Nanjing, China
Email:yang.wang@nju.edu.cn

***Abstract* – Interplanetary missions can benefit from the utilization of the Electric Delta-V Earth Gravity Assist (EDVEGA), a method that combines Delta-V Earth Gravity Assist with electric propulsion, validated by the Japanese asteroid explorer Hayabusa. Nevertheless, the early-phase inclusion of multi-body dynamics within the EDVEGA scheme remains incompletely explored. In this study, we present a methodology for integrating multi-body dynamics into the EDVEGA scheme by utilizing the resonant orbit as a first guess of an EDVEGA trajectory in the Circular Restricted Three-Body Problem (CRTBP) model. An indirect approach is employed to ascertain the minimum-fuel EDVEGA trajectories. Additionally, an efficient technique incorporating energy-to-fuel homotopy is embraced to enhance solutions search capabilities across broader domains of convergence. Through an examination of the achieved efficiency, we formulate an optimal strategy for interplanetary trajectory design and validate its efficacy through applications to missions to Jupiter and Saturn. In summary, the proposed resonance-based EDVEGA scheme demonstrates a notable enhancement in velocity requirements and is useful in practical cases.**

I. INTRODUCTION

Electric propulsion (EP) has emerged as a crucial technology for significantly lowering fuel consumption of space trajectories due to its high specific impulse. The importance of this technology has been demonstrated by several interplanetary missions, including Deep Space 1 [1], Hayabusa [2], Dawn [3], and BepiColombo [4]. Meanwhile, the concept of using gravity assists (but without electric propulsion) has been deliberated for decades and effectively applied to space missions [5-8]. Both electric propulsion and gravity assist techniques provide significant benefits in interplanetary missions compared to the Hohmann transfer or any more energetic transfer. In recent years, there has been a growing interest in the combination of high-specific-impulse, low-thrust propulsion with gravity assists for more challenging deep space explorations [9-12].

In particular, the so-called EDVEGA scheme that combines the Delta-V Earth Gravity Assist with low-thrust propulsion was proposed by Kawaguchi [13] and has been validated in the Japanese asteroid explorer Hayabusa [14]. The preliminary design of an EDVEGA trajectory often employs an analytical solution derived from Hill's equation [15-17], which describes the motion near Earth's orbit, accounting solely for the influence of the Sun's gravity. However, the incorporation of multi-body dynamics in the early stages of the EDVEGA scheme is significant but remains insufficiently explored. Additionally, the application of resonant orbits in the CRTBP model for deep space exploration has attracted increasing attention due to their unique characteristics [18-20]. Therefore, the objective of this work is to utilize the resonant periodic orbits in the CRTBP model as a first guess for an EDVEGA trajectory, aiming to design the resonance-based low-thrust, gravity-assist interplanetary trajectory.

In the resonance-based EDVEGA scheme, the Earth departure to Earth re-encounter phase is typically approached as a two-point boundary value problem (TPBVP), which can be tackled using various numerical methods. In this study, the optimal EDVEGA solution is resolved using an indirect method [21]. This method treats the TPBVP as a root-finding problem with analytical gradients, requiring a suitable initial guess for effective algorithmic performance. However, the lack of analytical solutions to the initial guesses in the CRTBP model creates an additional challenge that motivates us to employ several effective techniques to manage the problem's complexity. Initially, we use the numerical continuation method [22] to generate candidate resonant periodic orbits with perihelion or aphelion located within the Earth's hill region in the CRTBP model. These resonant periodic orbits with different resonance ratios provide many initial guesses for the EDVEGA trajectories that satisfy various requirements. Additionally, the energy-to-fuel homotopy [23] and analytical Jacobian [24] are employed to mitigate the high sensitivity of the solutions concerning the initial guesses. Finally, the proposed resonance-based EDVEGA scheme is demonstrated in hypothetical flyby missions to Jupiter and Saturn, respectively.

The structure of the paper is as follows. Section II presents the dynamical model and revisits the resonant periodic orbits. Section III outlines the derivation of the minimum-fuel problem for EDVEGA trajectory design. Section IV discusses the computational results and efficiency analysis, followed by the analysis of practical

examples. Finally, concluding remarks are provided in Section V.

II. Background

A. The Controlled Circular Restricted Three-Body Problem

The Circular Restricted Three-Body Problem (CRTBP) describes the motion of a massless particle, such as a spacecraft, under the gravitational influence of two massive primaries, P_1 and P_2, with respective masses m_1 and m_2 ($m_1 > m_2$). These two primaries move under mutual gravity on circular orbits around their common center of mass. The dynamics of the spacecraft are described within a rotating frame in normalized distance, mass, and time units. The Sun-Earth model is considered in this work, and the mass ratio μ is defined as $\mu = m_2/(m_1 + m_2)$, which is the only parameter in this system. In the rotating frame, the Sun and the Earth are fixed at coordinates $(-\mu, 0, 0)$ and $(1-\mu, 0, 0)$. In cases involving low-thrust control in the CRTBP model, the dynamics equations of the spacecraft are expressed as follows:

$$\dot{\boldsymbol{x}} = f(\boldsymbol{x}, \boldsymbol{\alpha}, u) \Longrightarrow \begin{bmatrix} \dot{\boldsymbol{r}} \\ \dot{\boldsymbol{v}} \\ \dot{m} \end{bmatrix} = \begin{bmatrix} \boldsymbol{v} \\ \boldsymbol{g}(\boldsymbol{r}) + \boldsymbol{h}(\boldsymbol{v}) + \dfrac{uT_{max}\boldsymbol{\alpha}}{m} \\ \dfrac{uT_{max}}{c} \end{bmatrix} \quad (1)$$

where $\boldsymbol{r} = (x, y, z)^T$, $\boldsymbol{v} = (\dot{x}, \dot{y}, \dot{z})^T$ denote the position and velocity vectors of the spacecraft, respectively. T_{max} represents the maximum thrust magnitude of the engine, u signifies the throttle factor, and m stands the mass of the spacecraft. $\boldsymbol{\alpha}$ denotes the unit vector in the direction of thrust. Additionally, $c = I_{sp} g_0$ denotes the exhaust velocity of the engine, in which I_{sp} represents the engine's specific impulse and g_0 is the gravitational acceleration. Table 1 reports the value of physical constants used in this study and the associated units of distance, time, and speed according to the normalization of the CRTBP. The expressions for $\boldsymbol{g}(\boldsymbol{r})$ and $\boldsymbol{h}(\boldsymbol{v})$ are defined as follows:

$$\boldsymbol{g}(\boldsymbol{r}) = \begin{bmatrix} \Omega_x \\ \Omega_y \\ \Omega_z \end{bmatrix} \quad \boldsymbol{h}(\boldsymbol{v}) = \begin{bmatrix} 2\dot{y} \\ -2\dot{x} \\ 0 \end{bmatrix} \quad (2)$$

where Ω is the pseudo-potential, defined as

$$\Omega = \frac{(x^2 + y^2)}{2} + \frac{1-\mu}{r_1} + \frac{\mu}{r_2} + \frac{\mu(1-\mu)}{2} \quad (3)$$

$$r_1 = \sqrt{(x+\mu)^2 + y^2 + z^2} \quad r_2 = \sqrt{(x-1+\mu)^2 + y^2 + z^2}$$

in which r_1 and r_2 are the distances from the spacecraft to the Sun and Earth, respectively. The Jacobi constant J_c is the first integral for the motion in CRTBP, defined as

$$J_c = 2\Omega - (\dot{x}^2 + \dot{y}^2) \quad (4)$$

Table 1. Physical constants used in this work.

Specific	Symbol	Value	Unit
Sun-Earth mass parameter	μ	3.0×10^{-6}	-
Distance unit	DU	149597900	km
Time unit	TU	5022523	s
Speed unit	VU	29.78540867	km/s
Hill sphere	r_{hill}	0.098	DU
Initial mass of the spacecraft	m_0	50	kg
Maximum thrust magnitude	T_{max}	0.001	N
Specific impulse	I_{sp}	3000	s
Standard gravity	g_0	9.80665	m/s^2

B. Resonant Periodic Orbits

In this study, resonant periodic orbits are utilized as an initial approximation for designing the EDVEGA trajectories. Within the two-body problem, an orbit-orbit resonance is defined by the ratio $p{:}q$ (where p and q are positive integers), with p indicating the period of motion for the spacecraft, and q representing the period of motion for the smaller primary [25]. When the spacecraft is in a $p{:}q$ resonance with Earth, it completes exactly p revolutions around the Sun within the same timeframe that Earth requires for q revolutions. Let T_p and T_q denote the orbital periods of the spacecraft and Earth, respectively, such that the ratio between periods is:

$$p{:}q = n_p{:}n_q = T_q{:}T_p \quad (5)$$

$$n_i = \sqrt{Gm_1/a_i^3} \quad (i = p \text{ or } q)$$

in which Gm_1 is the gravitational parameter of the Sun in the two-body model and a_i is the semi-major axis.

In the CRTBP model, the $p{:}q$ ratio does not precisely correspond to the ratio of the orbital periods associated with the bodies in resonance. Instead, in a $p{:}q$ resonance, the spacecraft completes *approximately* p revolutions around the Sun during the time it takes Earth to complete *roughly* q revolutions. Consequently, the ratio of orbital periods represents an *approximate* rational function rather than a strictly rational one. The inclusion of a third gravity field into the two-body model introduces perturbations to the trajectory, often resulting in orbits that are neither closed nor periodic. By employing the numerical continuation method [22], the resonant orbits within the CRTBP model maintain closed and display periodic trajectories, as observed in the rotating reference frame. Representative examples from various planar families of $p{:}q$ resonant orbits in the Sun-Earth system are illustrated in Fig. 1.

Our focus lies in selecting resonant orbits that closely approach Earth to take advantage of the effects of the Earth's gravity for interplanetary transfers. Therefore,

we select one orbit from each of the families shown in Fig. 1, resulting in a total of six resonant periodic orbits that serve as initial reference orbits for subsequent EDVEGA trajectory design. The selected orbits with resonance ratios of 2:1, 3:2, and 4:3 all have aphelion points within the Earth's hill region, while the selected orbits with resonance ratios of 1:2, 2:3, and 3:4 have periapsis points within the Earth's hill region. The hill spere r_{hill} that defines the hill region of the Earth in the Sun-Earth system is presented in Table 1. Moreover, the initial states $(x_0, 0, 0, 0, \dot{y}_0, 0)$ in the hill region and half orbital periods of the six selected resonant orbits are detailed in Table 2.

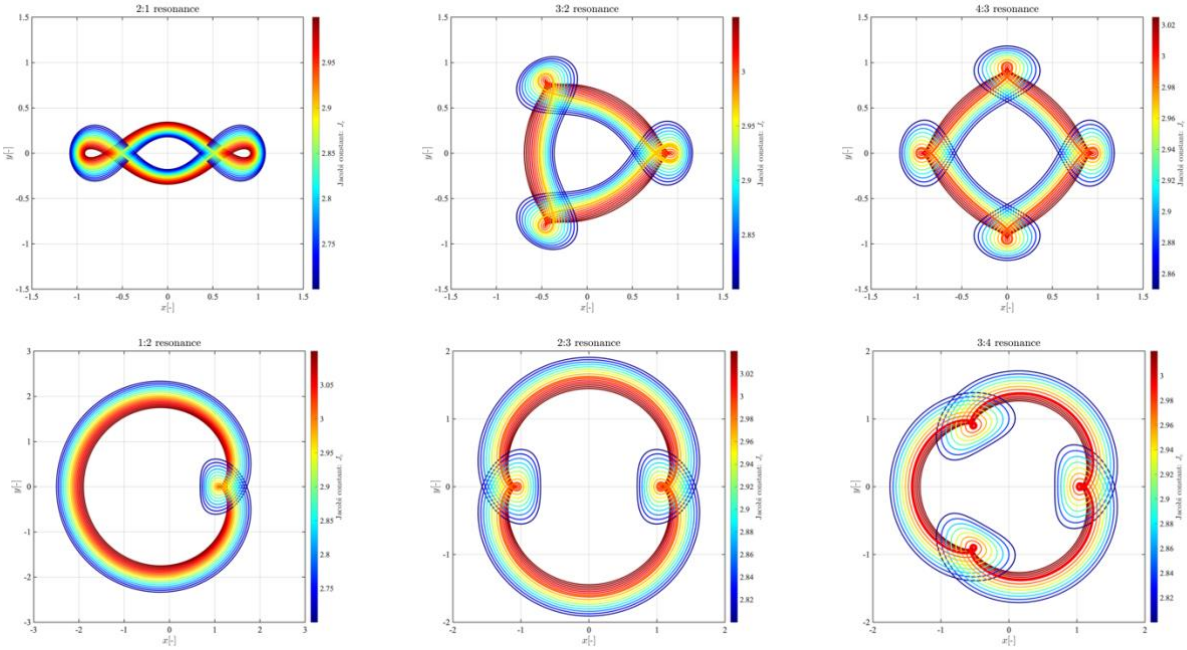

Fig. 1. Representative orbits in the planar p: q families, shown in the Sun-Earth rotating frame.

Table 2. Initials states of the six selected resonant orbits.

p: q	x_0 [-]	$\dot{y}_0$ [-]	$T/2$ [-]
2:1	0.993760130196872	-0.343262689922185	3.142993019924956
3:2	0.993074256652552	-0.156797751251266	6.289659432827232
4:3	0.993518754238172	-0.102047530366185	9.441091315716509
1:2	1.009686951107567	0.154262053153071	6.288780044897431
2:3	1.009409549218411	0.096803482225755	9.437998807822426
3:4	1.009323079230942	0.069009605267267	12.590538256801031

III. EDVEGA TRAJECTORY DESIGN

The resonance-based EDVEGA scheme is defined as follows. At the initial time t_i, the spacecraft is assumed to be in a resonant periodic orbit with initial states detailed in Table 2. At the final time t_f, the spacecraft will return to its initial position with a larger Earth-relatively velocity. The optimal control strategy for the resonance-based EDVEGA phase aims to maximize the Earth-relatively velocity at Earth re-encounter with minimum fuel consumption.

A. Problem Formulation

A performance index for the minimum-fuel problem is expressed as

$$J_f = \frac{T_{max}}{c} \int_{t_i}^{t_f} u \, dt \tag{6}$$

where t_i and t_f denote the initial and final times, respectively. The optimal control variables u and $\boldsymbol{\alpha}$ must satisfy the first-order necessary optimality conditions given by Pontryagin's Maximum Principle (PMP) [26]. In the minimum-fuel problem, u is either zero or one. To address the discontinuity resulting from the dichotomy of u, a homotopy method is employed [23], which establishes a connection between the energy-optimal problem and the fuel-optimal problem by introducing a homotopy parameter ε. The new

performance index to be minimized is

$$J_f = \frac{T_{max}}{c}\int_{t_i}^{t_f}[u - \varepsilon u(1-u)]\,dt \quad \varepsilon \in [0,1] \tag{7}$$

The Hamiltonian of the problem is:

$$H = \boldsymbol{\lambda}_r^T \cdot \boldsymbol{v} + \boldsymbol{\lambda}_v^T \cdot \left[\boldsymbol{g}(\boldsymbol{r}) + \boldsymbol{h}(\boldsymbol{v}) + \frac{uT_{max}\boldsymbol{\alpha}}{m}\right] - \lambda_m \frac{uT_{max}}{c} + \frac{T_{max}}{c}[u - \varepsilon u(1-u)] \tag{8}$$

where $\boldsymbol{\lambda} = (\boldsymbol{\lambda}_r, \boldsymbol{\lambda}_v, \lambda_m)^T$ is the vector of costates. The PMP provides expressions for the dynamics of the costate as:

$$\dot{\boldsymbol{\lambda}} = -\frac{\partial H}{\partial \boldsymbol{x}} \Longrightarrow \begin{bmatrix} \dot{\boldsymbol{\lambda}}_r \\ \dot{\boldsymbol{\lambda}}_v \\ \dot{\lambda}_m \end{bmatrix} = \begin{bmatrix} -\boldsymbol{G}_r^T\boldsymbol{\lambda}_v \\ -\boldsymbol{\lambda}_r - \boldsymbol{H}_v^T\boldsymbol{\lambda}_v \\ -\lambda_v \frac{uT_{max}}{m^2}\boldsymbol{\alpha} \end{bmatrix} \tag{9}$$

From PMP, the optimal control law minimizing the Hamiltonian H yields:

$$\boldsymbol{\alpha} = -\frac{\boldsymbol{\lambda}_v}{\lambda_v} \tag{10}$$

The optimal control throttle factor u depends on the switching function S, which is defined as:

$$S = -\lambda_v \frac{c}{m} - \lambda_m + 1 \tag{11}$$

as follows,

$$u = \begin{cases} 0 & if\ S > \varepsilon \\ (\varepsilon - S)/2\varepsilon & if\ -\varepsilon \le S \le \varepsilon \\ 1 & if\ S < -\varepsilon \end{cases} \tag{12}$$

Then, the motion can be integrated implicitly with dynamics:

$$\dot{\boldsymbol{y}} = F(\boldsymbol{y}) = \begin{bmatrix} \dot{\boldsymbol{r}} \\ \dot{\boldsymbol{v}} \\ \dot{m} \\ \dot{\boldsymbol{\lambda}}_r \\ \dot{\boldsymbol{\lambda}}_v \\ \dot{\lambda}_m \end{bmatrix} = \begin{bmatrix} \boldsymbol{v} \\ \boldsymbol{g}(\boldsymbol{r}) + \boldsymbol{h}(\boldsymbol{v}) + \frac{uT_{max}\boldsymbol{\alpha}}{m} \\ -\frac{uT_{max}}{c} \\ -\boldsymbol{G}_r^T\boldsymbol{\lambda}_v \\ -\boldsymbol{\lambda}_r - \boldsymbol{H}_v^T\boldsymbol{\lambda}_v \\ -\lambda_v \frac{uT_{max}\boldsymbol{\alpha}}{m^2} \end{bmatrix} \tag{13}$$

in which

$$\boldsymbol{G}_r = \frac{\partial \boldsymbol{g}(\boldsymbol{r})}{\partial \boldsymbol{r}} \quad \boldsymbol{H}_v = \frac{\partial \boldsymbol{h}(\boldsymbol{v})}{\partial \boldsymbol{v}} \tag{14}$$

The full set of boundary conditions and transversality conditions of this problem are:

$$\boldsymbol{\psi}(\boldsymbol{x}(t_f), t_f) = \begin{bmatrix} \boldsymbol{r}(t_f) - \boldsymbol{r}_i \\ |\boldsymbol{v}(t_f)| - |\boldsymbol{v}(t_i)| - \Delta v_{given} \end{bmatrix} = 0$$

$$\begin{bmatrix} \boldsymbol{\lambda}(t_f) - \left(\boldsymbol{\nu}^T \frac{\partial \boldsymbol{\psi}(\boldsymbol{x}_f, t_f)}{\partial \boldsymbol{x}}\right)^T \\ \boldsymbol{\nu}^T \frac{\partial \boldsymbol{\psi}(\boldsymbol{x}_f, t_f)}{\partial t} + H \end{bmatrix} = 0 \tag{15}$$

In equation (15), $\boldsymbol{v}_i$ and $\boldsymbol{v}_f$ are the initial and final velocity, respectively. Δv_{given} is the velocity increment at the Earth re-encounter. $\boldsymbol{\nu}$ is an additional unknown Lagrange multiplier corresponding to the final state constraints. In our study, the initial time is fixed to zero and the final time t_f is free. Therefore, this two-point boundary value problem can be transformed into an initial value problem aiming to determine the variables $(\boldsymbol{\lambda}_i, \boldsymbol{\nu}, t_f)$ such that the boundary conditions and the transversality conditions are satisfied. A shooting method is used to find the root of the shooting function in equation (15).

B. *Continuation and Solution Efficiency*

We initiate our analysis from the natural motions of resonant periodic orbits and progressively increase the velocity increment at Earth re-encounter, i.e., Δv_{given} to generate families of fuel-optimal EDVEGA trajectories. The computation of minimum-fuel solutions follows a three-step continuation process:

1) Using the low-thrust configuration provided in Table 1 and a predetermined $\Delta v_{given}(k)$, the minimum-energy problem ($\varepsilon = 1$) is solved iteratively.
2) Once an energy-optimal solution is reached, ε is gradually reduced until the minimum-fuel problem ($\varepsilon = 0$) is attained.
3) Once a fuel-optimal solution is obtained for $\Delta v_{given}(k)$, we further increase the velocity increment, i.e., proceed with $\Delta v_{given}(k+1) = \Delta v_{given}(k) + \delta v$ and repeat steps 1) and 2) to identify the new minimum-fuel solution.

During the continuation process, the costates exhibit high sensitivity within these highly nonlinear vector fields. Therefore, we employ both the adjoint control transformation (ACT) method and analytical derivatives for a local targeting search [24]. Our calculations demonstrate the high effectiveness of these two methods in the continuation process.

To further evaluate the characteristic of minimum-fuel EDVEGA families, we conduct a comprehensive investigation about the efficiency of the EDVEGA trajectories. Specifically, the velocity change during the EDVEGA phase is defined as [27]

$$\Delta v_{ega} = c \ln \frac{m_0}{m_f} \tag{16}$$

in which m_0 and m_f are the initial and final mass of the spacecraft, respectively. The efficiency of an EDVEGA trajectory is define as the ratio of the velocity increment from Earth departure to Earth re-encounter to the velocity consumption required by the low-thrust engine, i.e.,

$$efficiency = \frac{\Delta v_{given}}{\Delta v_{ega}} \tag{17}$$

IV. Simulations and Results

A. *Resonance-Based EDVEGA Families*

The six resonance-based minimum-fuel EDVEGA families are reported in Fig. 2 and 3. Each point in both figures is associated with an optimal solution with a fixed departure state that coincides with the six selected resonant periodic orbits in Table 2. In Fig. 2 and 3, the velocities are re-scaled using the speed units in Table 1. In Fig. 2, the horizontal axis represents the magnitude of the spacecraft's departure velocity v_i, while the vertical axis denotes the magnitude of the velocity at Earth re-encounter v_f. Fig. 3 shows the relationship between v_f and the velocity consumption during the EDVEGA phase Δv_{ega}. Different colors indicate the efficiency value corresponding to EDVEGA trajectories. The presence of family discontinuities in the two figures is due to the further constrained condition:

$$|v_f - (v_i + \Delta v_{given})| < 10^{-10}$$

It can be observed from Fig. 2 and 3 that the magnitude of the final velocity at Earth re-encounters for trajectories with resonance ratios of 2:3, 4:3, 1:2, and 3:2 can continue to extend from lower to higher values, indicating a significant increase in Earth-relative velocity due to the resonance-based EDVEGA scheme. In the case of the 3:4, 2:3, and 1:2 resonances, the efficiency at the onset of the family is notably high, suggesting that employing concise low-thrust arc segments along these resonant trajectories can markedly alter the relative velocity upon re-encounter near Earth. In general, the efficiency of the EDVEGA trajectories decreases with the increasing velocity at the Earth re-encounter. Besides, the final velocity increments for the 3:4 and 2:1 resonance exhibit a relatively minor increase. In the case of 2:1 resonance, the resonance-based EDVEGA family divides into two segments, where despite variations in velocity increments, the difference in efficiency is not significant. Table 3 presents the maximum v_f that can be achieved using the six resonant periodic orbits, along with the corresponding Δv_{ega} and their efficiency values.

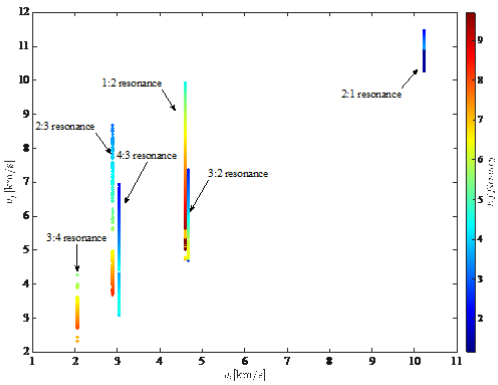

Fig. 2. Resonance-based EDVEGA families, shown in (v_i, v_f) plane. Different colors indicate the efficiency values.

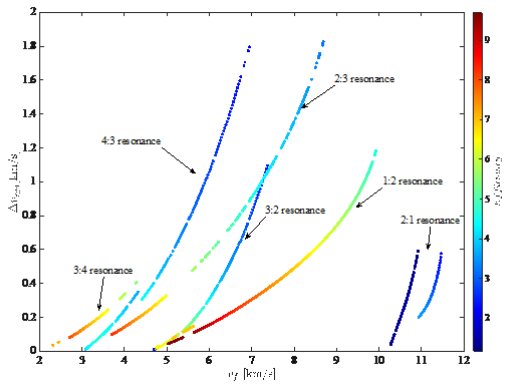

Fig. 3. Resonance-based minimum-fuel EDVEGA families, shown in $(v_f, \Delta v_{ega})$ plane. Different colors indicate the efficiency values.

Table 3. Maximum v_f along with Δv_{ega} and efficiency values in resonance-based EDVEGA family.

$p:q$	v_f (km/s)	Δv_{ega}(km/s)	efficiency
2:1	11.4642	0.5771	2.1485
3:2	7.3702	1.0955	2.4644
4:3	6.9395	1.7951	2.1725
1:2	9.9247	1.1845	4.4998
2:3	8.6833	1.8250	3.1780
3:4	4.2855	0.4082	5.4623

B. *Examples of Minimum-Fuel Solutions*

We utilize the 2:3 resonance as a case study, selecting three sample $\Delta v_{given}s$ to demonstrate the minimum-fuel resonance-based EDVEGA trajectories in both the Sun-Earth rotation frame (Fig. 4) and the Sun-centered inertial frame (Fig. 5) with dimensionless distance unit (see Table 1). In both figures, the blue and red lines indicate thrust and coast arcs, respectively. Notably, in the minimum-fuel resonance-based EDVEGA solutions, the thruster is on duty mainly across the periapsis and apoapsis. Meanwhile, as illustrated in Fig. 4 and 5, the duration of the thrust arcs extends with increasing Δv_{given}. The thrust profile T, switching function trends S, and the mass of spacecraft along the trajectories are reported in Fig. 6. Overall, the ability of the continuation process in smoothing and the thrust profile is evident. These optimal solutions adhere to the principle in optimal control theory, ensuring continuous trajectories and demonstrating the robustness of current algorithms.

Table 4. Parameters of example minimum-fuel solutions shown in Fig. 4-6.

	Δv_{given}(km/s)	Δv_f(km/s)	efficiency
Case-1	3.0700	5.9533	5.3881
Case-2	4.5800	7.4633	4.1814
Case-3	5.7900	8.6733	3.1895

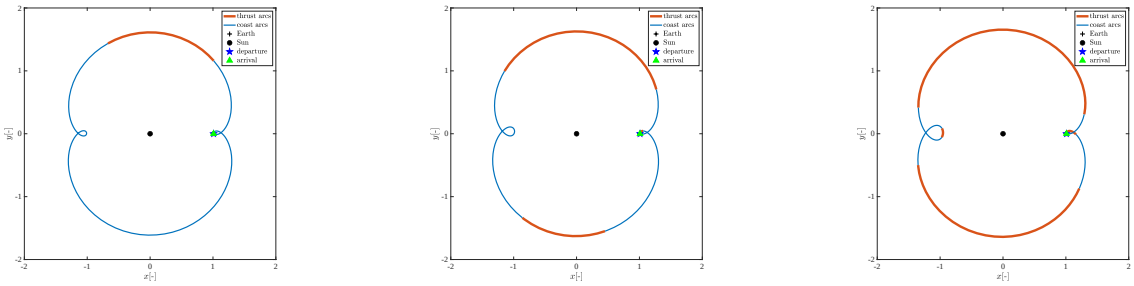

Fig. 4. Resonance-based EDVEGA trajectories for different values of Δv_{given} (see Table 4).
Left: case-1; Middle: case-2; Right: case-3, shown in Sun-Earth rotating frame.

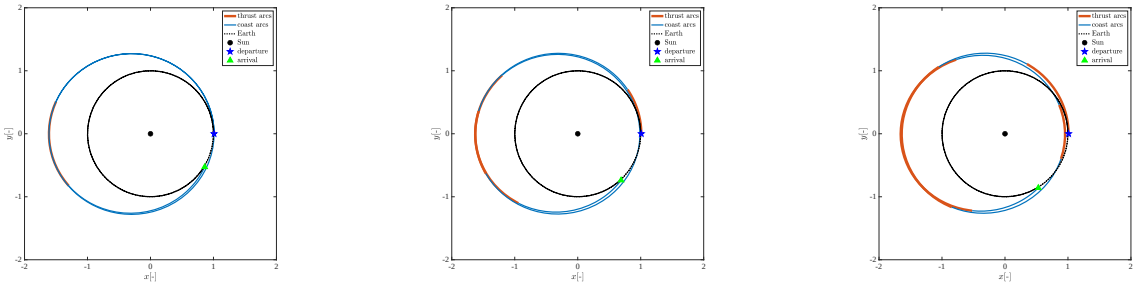

Fig. 5. Resonance-based EDVEGA trajectories for different values of Δv_{given} (see Table 4).
Left: case-1; Middle: case-2; Right: case-3, shown in Sun-centered inertial frame.

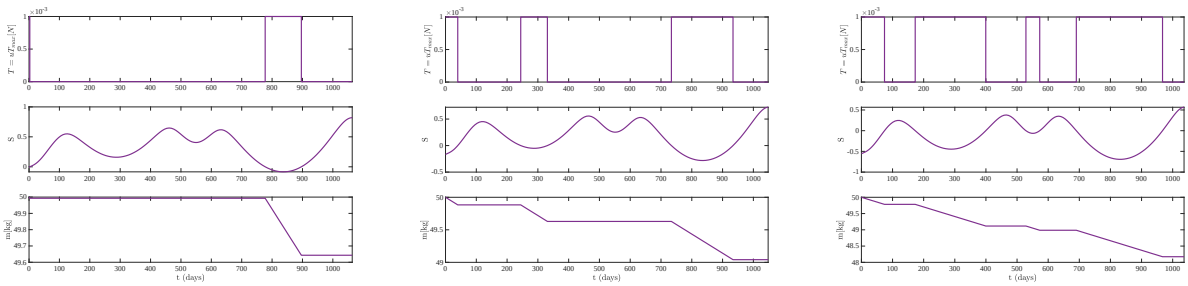

Fig. 6. Thrust T, switching function S , and the spacecraft's mass m of
the minimum-fuel solutions shown in Fig. 4 and 5.

C. *Flyby Mission Examples*

Jupiter and Saturn are chosen as targets for further analysis. Utilizing the resonance-based EDVEGA scheme proposed in the previous section, we illustrate flyby trajectories from Earth to Jupiter and Saturn. Initially, the ballistic Earth-Jupiter and Earth-Saturn transfer trajectories are computed by solving Lambert's problem. The timing of the Lambert transfer departure aligns with Earth's re-encounter in the EDVEGA phase, set within the range of [2029/01/01 2030/06/30]. The duration of transfers is bounded between 800 and 1200 days for the Earth-Jupiter (E-J) mission, and 1500 and 2500 days for the Earth-Saturn (E-S) mission. The positions and velocities of Earth, Jupiter, and Saturn are determined by the Jet Propulsion Laboratory's ephemeris DE405. Table 5 lists the optimal Lambert transfer parameters within the specific time frame, including the departure date (T1), arrival date (T2), transfer duration (TOF), and the required Earth's relative velocity V_∞ at the departure date.

Table 5. Parameters of optimal Lambert trajectories.

	T1 (UTC)	T2 (UTC)	TOF (year)	V_∞ (km/s)
E-J	2030-01-21	2032-05-12	2.3068	8.7712
E-S	2029-07-20	2034-06-27	4.9397	10.3437

Table 6. Parameters of EDVEGA trajectories.

	V_∞ (km/s)	Δv_{ega} (km/s)	Efficiency	Δm(kg)
E-J	8.7748	0.06764	6.18	1.1364
E-S	10.3442	0.0887	1.3522	0.1506

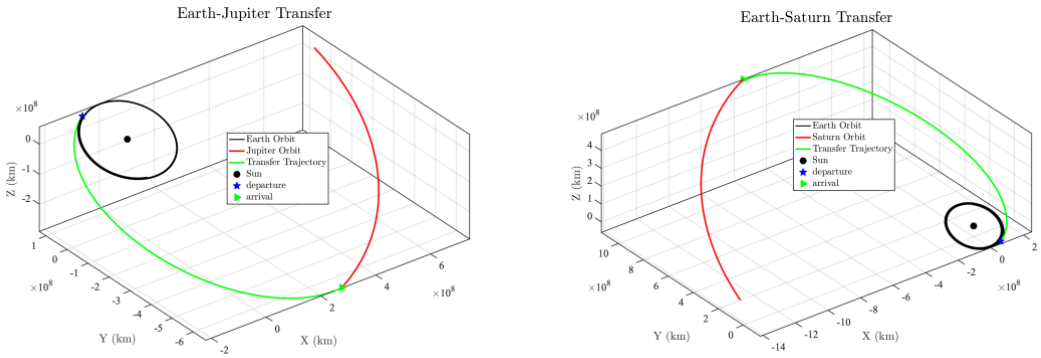

Fig. 7. Lambert transfer trajectory with the optimal Earth departure velocity. Left: Sun-Jupiter transfer. Right: Sun-Saturn transfer, shown in Sun-centered inertial frame.

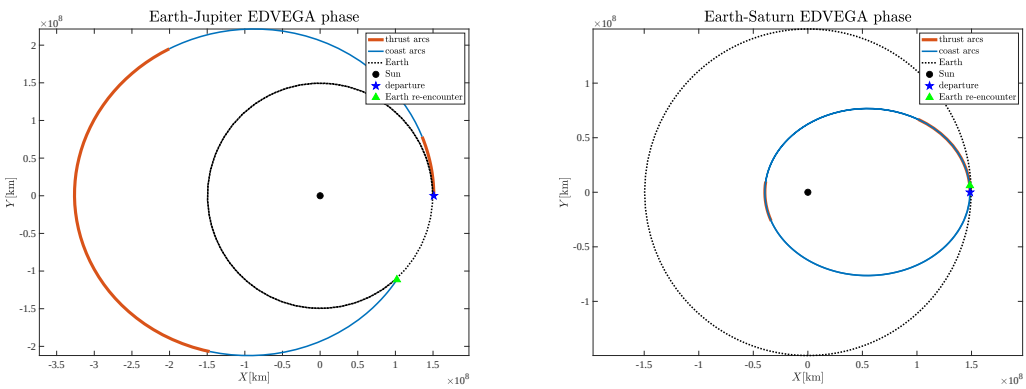

Fig. 8. EDVEGA phase for optimal Lambert transfers. Left: Sun-Jupiter EDVEGA phase. Right: Sun-Saturn EDVEGA phase, shown in Sun-centered inertial frame.

Based on the minimum Earth departure velocity requirements provided by the Lambert transfers, we identify the minimum-fuel trajectories capable of meeting the velocity criteria for the Earth-Jupiter transfer and the Earth-Saturn transfer within the 1:2 and 2:1 resonance-based EDVEGA families, respectively. Table 6 displays the Earth-relative velocity at the Earth re-encounter during the EDVEGA phase V_∞, the velocity requirement of low-thrust arcs Δv_{ega}, the efficiency of the EDVEGA trajectories, and the mass consumption for these two missions. The related trajectories are shown in Fig. 7 and 8. From the EDVEGA families generated in the previous section, it is evident that selecting the minimum-fuel solutions satisfying the necessary Earth-relative departure velocity is straightforward and efficient.

V. Conclusion

In this work, the resonance-based Electric Delta-V Earth Gravity Assist (EDVEGA) scheme is proposed for preliminary analysis of interplanetary missions. The low-thrust minimum-fuel problem is considered in the circular restricted three-body problem using indirect optimal control. Techniques such as the numerical continuation of resonant periodic orbits, energy-to-fuel homotopy, and analytical derivative are employed to mitigate the challenges posed by the strong sensitivity of the dynamics. As a result, a large number of minimum-fuel EDVEGA trajectories have been found and their effectiveness is evaluated in hypothetical Jupiter and Saturn flyby missions.

The following step of the study will be to compute more resonance-based EDVEGA families with different resonance ratios to expand the database while considering combinations of different resonances to further improve the efficiency of the EDVEGA trajectories.

Acknowledgements

The work of the second author was partially supported by Japan Science and Technology Agency, Fusion Oriented Research for Disruptive Science and Technology (JST FOREST Program), Grant Number JPMJFR206M and Grant-in-Aid for Scientific Research from the Japan Society for the Promotion of Science, Grant Number 22H03663.

VI. References

[1] M. D. Rayman, P. Varghese, D. H. Lehman, L. L. Livesay, "Results from the Deep Space 1 technology validation mission", *Acta Astronautica*, vol. 47(2), pp. 475–487, July 2000.

[2] J. Kawaguchi, A. Fujiwara, T. Uesugi, "Hayabusa-Its technology and science accomplishment summary and Hayabusa-2", *Acta Astronautica*, vol. 62(10), pp. 639–647, May 2008.

[3] C. T. Russell, M. A. Barucci, R. P Binzel, M. Capria, U. Christensen, A. Coradini, M. De Sanctis, W. Feldman, et al., "Exploring the asteroid belt with ion propulsion: Dawn mission history, status and plans", *Advances in Space Research*, vol. 40(2), pp. 193–201, December 2007.

[4] P. N. Randall, R. A. Lewis, S. D. Clark, K. K. Chan, H. Gray, F. Striedter, C. Steiger, "BepiColombo-MEPS commissioning activities and T6 ion thruster performance during early mission operations", in *Proceedings of the 36th International Electric Propulsion Conference*, Vienna, Austria, September 15-20, 2019.

[5] J. C. Niehoff, "Gravity-assisted trajectories to solar system targets", *Journal of Spacecraft and Rockets*, vol. 3(9), pp. 1351-1356, September 1966.

[6] M. A. Minovitch, "Gravity thrust Jupiter orbiter trajectories generated by encountering the Galilean satellites", *Journal of Spacecraft and Rockets*, vol. 9(10), pp. 751-756, November 1972.

[7] S. J. Matousek, "The Juno new frontiers mission", *Acta Astronautica*, vol. 61(10), pp. 932–939, November 2007.

[8] S. K. Matsumoto, "Voyager interstellar mission: Challenges of flying a very old spacecraft on a very long mission", in *Proceedings of the 14th International Conference on Space Operations*, Daejeon, Korea, 2016.

[9] S. N. Williams, V. Coverstone, "Benefits of solar electric propulsion for the next generation of planetary exploration missions", *Journal of the Astronautical Sciences*, vol. 45(2), pp. 143-159, April 1997.

[10] C. H. Yam, T. T. McConaghy, K. J. Chen, J. M. Longuski, "Design of low-thrust gravity-assist trajectories to the outer planets", in *Proceedings of the 55th International Astronautical Congress*, Vancouver, Cananda, 2004.

[11] M. Okutsu, C. H. Yam, J. M. Longuski, "Low-thrust trajectories to Jupiter via gravity assists from Venus, Earth, and Mars", in *Proceedings of the AIAA/AAS Astrodynamics Specialist Conference and Exhibit*, Keystone, Colorado, August 2006.

[12] Y. Shimane, K. Ho, "Gravity-assist low-thrust inter-system trajectory design with manifold captures", *Journal of the Astronautical Sciences*, vol. 69(2), pp. 193-217, April 2022.

[13] J. Kawaguchi, "Solar electric propulsion leverage: Electric Delta-VEGA (EDVEGA) scheme and its application", in *Proceedings of the 11th AAS/AIAA Space Flight Mechanics meeting*, Santa Barbara, California, 2001.

[14] J. Kawaguchi, H. Kuninaka, A. Fujiwara, T. Uesugi, "MUSES-C, Its launch and early orbit operations", *Acta Astronautica*, vol. 59, pp. 669-678, Octorber 2006.

[15] T. Ikenaga, M. Utashima, N. Ishii, Y. Kawakatsu, M. Yoshikawa, "Interplanetary parking method and its applications", *Acta Astronautica*, vol. 116, pp. 271–281, November 2015.

[16] D. Tamakoshi, H. Kojima, "Set-oriented design of interplanetary low-thrust trajectories using Earth Gravity Assist", *Acta Astronautica*, vol. 156, pp. 208-218, March 2019.

[17] Y. Takao, O. Mori, M. Matsushita, A. K. Sugihara, "Solar electric propulsion by a solar power sail for small spacecraft missions to the outer solar system", *Acta Astronautica*, vol. 181, pp. 362-376, April 2021.

[18] M. Vaquero, K. Howell, "Leveraging resonant-orbit manifolds to design transfers between libration-point orbits", *Journal of Guidance, Control, and Dynamics,* vol. 37(4), pp. 1143-1157, 2014.

[19] S. Pan, X. Hou, "Analysis of resonance transition periodic orbits in the circular restricted three-body problem", *Applied Sciences*, vol. 12(18), September 2022.

[20] A. Wilmer, R. Bettinger, M. J. Holzinger, J. A. Dahlke, "Sun–Venus CR3BP, part 1: periodic orbit generation, stability, and mission investigation", *Archive of Applied Mechanics*, vol. 94(1), pp. 1-21, March 2024.

[21] C. Zhang, F. Topputo, F. Bernelli-Zazzera, Y. S. Zhao, "Low-thrust minimum-fuel optimization in the circular restricted three-body problem", *Journal of Guidance, Control, and Dynamics*, vol. 38(8), pp. 1-9, March 2015.

[22] M. Lara, J. Peláez, "On the numerical continuation of periodic orbits. An intrinsic, 3-dimensional, differential, predictor-corrector algorithm", *Astronomy and Astrophysics*, vol. 389, pp. 692–701, 2002.

[23] T. Haberkorn, P. Martinon, J. Gergaud, "Low thrust minimum-fuel orbital transfer: a homotopic approach", *Journal of Guidance, Control, and Dynamics*, vol. 27(6), 2004.

[24] R. P. Russell, "Primer vector theory applied to global low-thrust trade studies", *Journal of Guidance, Control, and Dynamics*, vol. 30(2), pp. 460-472, March 2007.

[25] C. D. Murray, S. F. Dermott, "Solar System Dynamics", *Cambridge Univ. Press*, Cambridge, England, U.K., 1999, pp. 321–333.

[26] A. Bryson, Y. C. Ho, "Applied Optimal Control: Optimization, Estimation and Control", *Halsted Press book*. Taylor & Francis, New York, 1975.

[27] H. D. Curtis, "Orbital Mechanics for Engineering Students", *Orbital Mechanics for Engineering Students*, pp. 1-751, 2013.